Nonlinearly driven second harmonics of Alfvén cascades

H. Smith
Department of Radio and Space Science, Chalmers University of Technology, SE-412 96 Göteborg, Sweden

B. N. Breizman
Institute for Fusion Studies, The University of Texas at Austin, Austin, Texas 78712

M. Lisak and D. Anderson
Department of Radio and Space Science, Chalmers University of Technology, SE-412 96 Göteborg, Sweden

(Received 20 December 2005; accepted 3 March 2006; published online 18 April 2006)

In recent experiments on Alcator C-Mod [J. A. Snipes *et al.*, Phys. Plasmas **12**, 056102 (2005)], measurements of density fluctuations with phase contrast imaging through the plasma core show a second harmonic of the basic Alfvén cascade (AC) signal. The present paper presents a theory that describes the second-harmonic perturbation as a nonlinear sideband produced by the AC eigenmode via quadratic terms in the magnetohydrodynamic equations. It is shown that in a low-pressure plasma the nonlinear coupling to compressional Alfvén and acoustic perturbations can be neglected when calculating the second-harmonic density. The derived expressions for this density perturbation can potentially be used together with experimental measurements to determine the AC amplitude inside the plasma, rather than just at the edge as with magnetic probes. © *2006 American Institute of Physics*. [DOI: 10.1063/1.2192500]

I. INTRODUCTION

Alfvén cascades (ACs) have been observed in reversed shear operation of JT-60U,[1] the Joint European Torus,[2] and the Tokamak Fusion Test Reactor.[3] These eigenmodes are interpreted theoretically in Refs. 4 and 5 as shear Alfvén eigenmodes localized around the minimum q surface, and were later also named reversed shear Alfvén eigenmodes (RSAE) in other works.[6] The AC eigenmode frequency ω is slightly higher than the local maximum of the Alfvén continuum, $\omega_{\mathrm{A}m,n}=k_{\|}v_{\mathrm{A}}=(m-nq_{\star})v_{\mathrm{A}}/Rq_{\star}$, where $q_{\star}$ is the minimum q value, v_{A} is the Alfvén velocity, R is the major radius, and m and n are the poloidal and toroidal mode numbers, respectively.

In recent experiments on Alcator C-Mod,[7] measurements of density fluctuations with phase contrast imaging through the plasma core show a second harmonic of the fundamental AC perturbation. The aim of the present work is to evaluate the second-harmonic density perturbation produced by a given AC eigenmode via nonlinear terms in the momentum balance and continuity equations. This analysis of Alfvén cascade eigenmodes and their nonlinear sidebands should not be confused with turbulent cascades of Alfvén waves discussed in the literature (see, e.g., Ref. 8). For the sake of simplicity, the analysis is limited to the case of a plasma with low-pressure ($\beta=0$) and large aspect ratio ($\epsilon\ll 1$), for eigenmodes with large poloidal mode numbers ($m\gg 1$). To be able to interpret the laser interferometric measurements conclusively, one has to consider the specific laser path and estimate the nonlinearities introduced by the measurement. These measurement-specific aspects require additional investigation, and will be addressed in a future publication.

The second-harmonic perturbation at 2ω is nearly resonant with the $2m,2n$ branch of the Alfvén continuum $\omega_{\mathrm{A}2m,2n}$. The resulting enhancement of the second harmonic is counteracted by the relatively weak nonlinearity of the shear Alfvén wave. For shear Alfvén perturbations in a uniform equilibrium magnetic field, the quadratic terms $4\pi\rho(\mathbf{v}\cdot\nabla)\mathbf{v}$ and $(\mathbf{B}\cdot\nabla)\mathbf{B}$ tend to cancel in the momentum balance equation. For this reason, extreme care is needed to properly include magnetic curvature effects and to evaluate the coupling between shear Alfvén perturbations and compressional perturbations.

II. THE STRUCTURE OF THE PROBLEM

The AC mode is dominated by a single poloidal component in the Fourier representation of the perturbation. This part of the mode structure is known from linear theory (see Refs. 4 and 5), and is assumed to be given. The main part of the plasma displacement in an AC mode is incompressible, which makes it necessary to keep track of small compressional displacements in calculations of both linear and nonlinear contributions to the perturbed density. Coupling between different plasma displacement components (or equivalently, plasma velocity components) is determined by the momentum balance equation. Once all relevant perturbed velocities are derived for both the first and second harmonics, the density perturbation can be calculated via the continuity equation.

Let all quantities X (which can stand for magnetic field $\mathbf{B}$, velocity $\mathbf{v}$, density ρ, etc.) be represented as

$$X = X_0 + \sum_{l=1}^{\infty} X_l + \text{c.c.}, \tag{1}$$

where X_0 is the equilibrium part, and $X_l \propto \exp(-li\omega t)$ are the perturbed parts. We assume that $X_0 \gg X_1 \gg X_l$ for $l \neq 1$, which prevents any nonlinear feedback from the 2ω perturbation to the fundamental mode at the basic frequency ω.

The plasma velocity has three degrees of freedom, which can be represented by three scalar functions, ξ, Φ, and Ψ through

$$\mathbf{v} \equiv \dot{\xi}\mathbf{b}_0 + \frac{\mathbf{b}_0}{B_0} \times \nabla\dot{\Phi} + \frac{1}{B_0}\nabla_\perp \dot{\Psi}, \tag{2}$$

where B_0 is the magnitude and $\mathbf{b}_0$ the direction of the equilibrium magnetic field, and an overhead dot denotes a partial time derivative. Through this representation, one can distinguish between the acoustic (ξ), shear (Φ), and compressional (Ψ) velocity perturbations. Generally, in a first-order perturbation analysis of a uniform plasma with straight magnetic field lines, Φ corresponds to the scalar potential and Ψ is related to the perpendicular component of the vector potential, provided that a suitable gauge is chosen. In a curved magnetic field with second-order perturbations taken into account, this physical interpretation of Φ and Ψ in terms of the potentials is no longer valid; nevertheless, it is still possible to use the velocity representation of Eq. (2).

It should be pointed out that plasma pressure effects on Alfvén cascades are limited to the lowest frequencies of their sweeping interval.[9] The AC is virtually insensitive to plasma pressure in the rest of its frequency interval, which allows us to treat that part in the zero-pressure limit neglecting the plasma pressure in the perturbed momentum balance equation. It is convenient to apply the time derivative operator to the momentum balance equation, after which the first- and second-harmonic components become

$$4\pi\rho_0\ddot{\mathbf{v}}_1 - (\nabla \times \mathbf{B}_0) \times \nabla \times (\mathbf{v}_1 \times \mathbf{B}_0) - [\nabla \times \nabla \times (\mathbf{v}_1 \times \mathbf{B}_0)] \times \mathbf{B}_0 = 0, \tag{3}$$

$$\begin{aligned} &4\pi\rho_0\ddot{\mathbf{v}}_2 - (\nabla \times \mathbf{B}_0) \times \nabla \times (\mathbf{v}_2 \times \mathbf{B}_0) - [\nabla \times \nabla \times (\mathbf{v}_2 \times \mathbf{B}_0)] \times \mathbf{B}_0 \\ &= (\nabla \times \mathbf{B}_0) \times \nabla \times (\mathbf{v}_1 \times \mathbf{B}_1) + [\nabla \times \nabla \times (\mathbf{v}_1 \times \mathbf{B}_1)] \times \mathbf{B}_0 + \frac{\partial}{\partial t}\Big[-4\pi\rho_0(\mathbf{v}_1 \cdot \nabla)\mathbf{v}_1 + (\mathbf{B}_1 \cdot \nabla)\mathbf{B}_1 - 4\pi\rho_1\dot{\mathbf{v}}_1 \\ &\quad - \frac{1}{2}\nabla(\mathbf{B}_1 \cdot \mathbf{B}_1)\Big], \end{aligned} \tag{4}$$

where $\dot{\mathbf{B}}_1 = \nabla \times (\mathbf{v}_1 \times \mathbf{B}_0)$. The right-hand side of Eq. (4), containing all quadratic terms in $\mathbf{v}_1$, represents a driving force determining the second-harmonic velocity $\mathbf{v}_2$ through the linear operator on the left-hand side.

The vector equations [(3) and (4)] can each be split up into three scalar equations by applying the three operations

$$\begin{aligned} &\mathbf{b}_0 \cdot \{\text{Eq. (3) or (4)}\}, \\ &\nabla \cdot [\mathbf{b}_0/B_0 \times \{\text{Eq. (3) or (4)}\}], \\ &\nabla \cdot [1/B_0\{\text{Eq. (3) or (4)}\}_\perp], \end{aligned} \tag{5}$$

which produce the acoustic, vorticity, and compressional equations, respectively. This transforms Eqs. (3) and (4) into six equations, which can be written symbolically as

$$\text{Eq. (3)} \Leftrightarrow L^{1\alpha} = 0, \tag{6}$$

$$\text{Eq. (4)} \Leftrightarrow L^{2\alpha} = S^\alpha, \tag{7}$$

where the superscript α=a, v, and c indicates the acoustic, vorticity, and compressional equations, respectively. Equations (6) and (7) can be written as sums over contributions from the different velocity components,

$$\begin{aligned} &L^{1\alpha} \equiv \sum_{i=\Phi_1,\Psi_1,\xi_1} L_i^{1\alpha}, \quad L^{2\alpha} \equiv \sum_{i=\Phi_2,\Psi_2,\xi_2} L_i^{2\alpha}, \\ &S^\alpha \equiv \sum_{i,j=\Phi_1,\Psi_1,\xi_1} S_{ij}^\alpha. \end{aligned} \tag{8}$$

For example, $S^{\mathrm{a}}_{\Phi_1\Psi_1}$ represents the parallel projection (i.e., acoustic component) of the terms on the right-hand side of Eq. (4) that are bilinear in Φ_1 and Ψ_1. We do not distinguish between different orders of the two indices i and j (e.g., $S^{\mathrm{a}}_{\Phi_1\Psi_1} = S^{\mathrm{a}}_{\Psi_1\Phi_1}$). Equations (6) and (7) will be examined in detail in the following sections, and the dominating contributions to the second-harmonic density perturbation ρ_2 will be identified.

The density perturbation is related to $\mathbf{v}_1$ and $\mathbf{v}_2$ by the first- and second-harmonic components of the continuity equation

$$\dot{\rho}_1 = -\nabla \cdot (\rho_0 \mathbf{v}_1), \tag{9}$$

$$\dot{\rho}_2 = -\nabla \cdot (\rho_1 \mathbf{v}_1) - \nabla \cdot (\rho_0 \mathbf{v}_2). \tag{10}$$

The first term on the right-hand side of Eq. (10) is generated by the nonlinearity of the continuity equation, while the second term is generated by nonlinearities in the momentum balance equation [(4)]. The density ρ_2 can also be written in terms of the partial contributions from ξ_1, Φ_1, Ψ_1, ξ_2, Φ_2, and Ψ_2 as

$$\rho_2 = \rho_{\Phi_1^2} + \rho_{\Psi_1^2} + \rho_{\xi_1^2} + \rho_{\Phi_1\Psi_1} + \rho_{\Phi_1\xi_1} + \rho_{\Psi_1\xi_1} + \rho_{\xi_2} + \rho_{\Phi_2} + \rho_{\Psi_2}. \tag{11}$$

The first six of these contributions to the density perturbation come from the first term in Eq. (10), and the last three contributions come from the second term. To determine which of the nine terms in Eq. (11) that dominates, we will begin by deriving the first- and second-harmonic plasma velocity components from Eqs. (6) and (7).

III. FIRST-HARMONIC VELOCITY PERTURBATION

The first-harmonic equations [(6)] are

$$L^{1\mathrm{a}} = L^{1\mathrm{a}}_{\xi_1} = -4\pi\rho_0\omega^2\xi_1 = 0, \tag{12}$$

$$L^{1\mathrm{c}} = L^{1\mathrm{c}}_{\Psi_1} + L^{1\mathrm{c}}_{\Phi_1} = -\nabla \cdot \frac{1}{B_0}(\nabla\nabla \cdot (B_0 \nabla \Psi_1) + [(\nabla F_1 \cdot \nabla)\mathbf{B}_0 - (\mathbf{B}_0 \cdot \nabla)\nabla F_1] \times \mathbf{B}_0) = 0, \tag{13}$$

$$L^{1\mathrm{v}} = L^{1\mathrm{v}}_{\Phi_1} = \nabla \cdot \left(\frac{\omega^2}{v_{\mathrm{A}}^2}\nabla_\perp \Phi_1\right) + (\mathbf{B}_0 \cdot \nabla)\frac{1}{B_0^2}\nabla \cdot (B_0^2 \nabla_\perp F_1) - \nabla^2 \mathbf{B}_0 \cdot \nabla F_1 = 0, \tag{14}$$

where $F_1 \equiv \mathbf{b}_0/B_0 \cdot \nabla\Phi_1$. Because of the β=0 assumption,

Eq. (12) immediately yields $\xi_1=0$, which implies that $\rho_{\xi_1^2}=\rho_{\Psi_1\xi_1}=\rho_{\Phi_1\xi_1}=0$. Furthermore, Eq. (13) can be used together with $(\mathbf{b}_0\cdot\nabla)\sim k_\parallel\sim 1/(Rq)$, to obtain the estimate

$$\Psi_1\sim\frac{\varepsilon^2}{m^2q^2}\Phi_1, \tag{15}$$

which yields

$$\rho_{\Phi_1\Psi_1}\sim\frac{m^2}{r^2R^2q^2}\frac{\rho_0}{B_0^2}\Phi_1^2,\quad \rho_{\Psi_1^2}\sim\frac{1}{R^4q^4}\frac{\rho_0}{B_0^2}\Phi_1^2. \tag{16}$$

Let us now review the eigenmode analysis for Alfvén cascades to establish the radial profile $\tilde{\Phi}_1$ of the shear perturbation $\Phi_1\equiv\tilde{\Phi}_1(r)e^{i(n\varphi-m\theta-\omega t)}$, where $d\tilde{\Phi}_1/dr\sim(m/r)\tilde{\Phi}_1$. The eigenmode equation for $\tilde{\Phi}_1(r)$ follows from Eq. (14) and takes the form

$$\frac{1}{r}\frac{d}{dr}\left(rD\frac{d\tilde{\Phi}_1}{dr}\right)-\frac{m^2}{r^2}\tilde{\Phi}_1D=0, \tag{17}$$

where $D\equiv\omega^2/\bar{v}_A-\bar{k}_\parallel^2$, and a bar denotes a flux surface average.

Equation (17) is oversimplified because it does not include the hot ion contribution and higher-order toroidal corrections. The reason why these additional terms are essential is that they shift the eigenmode from the Alfvén continuum. In what follows, we add these terms to Eq. (17), taking their explicit form from Ref. 5. We also introduce a normalized coordinate $x\equiv(r-r_\star)m/r_\star$ and Taylor expand $\bar{k}_\parallel$ around the zero shear point $r=r_\star$ where the AC is located. After these steps, we find the amended Eq. (17) to be

$$\frac{d}{dx}(S+x^2)\frac{d\tilde{\Phi}_1}{dx}-(S+x^2)\tilde{\Phi}_1+Q_1\tilde{\Phi}_1=0, \tag{18}$$

where

$$S\equiv\frac{2(\omega-\omega_{Am,n})\omega_{Am,n}}{\bar{v}_A^2}\frac{mq_\star}{r_\star^2q_\star''}\frac{\bar{R}^2q_\star^2}{m-nq_\star}, \tag{19}$$

and prime denotes an r derivative. The coefficient Q_1 in Eq. (18) describes the effects of hot ions and toroidicity in the same way as in Ref. 5, i.e.,

$$Q_1=Q_{hot}+Q_{tor}\equiv\omega_{Am,n}^2\frac{q_\star^2\bar{R}^2}{\bar{v}_A^2(m-nq_\star)}\frac{q_\star}{r_\star^2q_\star''}\times\left[\frac{\omega_{ch}}{\omega_{Am,n}}\left(-\frac{r}{\rho}\frac{d\bar{\rho}_{hot}}{dr}\right)_{r=r_\star}+\frac{2m\varepsilon_\star(\varepsilon_\star+2\Delta_\star')}{1-4(m-nq_\star)^2}\right]. \tag{20}$$

In this expression, $\bar{\rho}_{hot}$ is the flux surface averaged hot ion density and Δ is the Shafranov shift. As shown in Refs. 4 and 5, Q_1 has to be greater than 1/4 for an eigenmode to exist. By introducing a new unknown function, $G_1(x)=\tilde{\Phi}_1(x)\sqrt{S+x^2}$, and using a variational approach with the ansatz $G_1=A\exp[-x^2/(2a^2)]$, we obtain for $Q_1=1$ an approximate solution with the following parameters: $a=1.247$ and $S=0.0983$. This result agrees with the lowest-order radial eigenmode found in Ref. 4.

Now we are in a position to estimate the Φ_1 contribution to ρ_2 through the quadratic nonlinearity in the continuity equation,

$$\rho_{\Phi_1^2}\simeq\left(\left[\frac{\mathbf{b}_0}{B_0}\times\nabla\Phi_1\right]\cdot\nabla\right)\left[\rho_0\nabla\Phi_1\cdot\left(\nabla\times\frac{\mathbf{b}_0}{B_0}\right)\right]\sim\frac{m^2}{r^3R}\frac{\rho_0}{B_0^2}\Phi_1^2. \tag{21}$$

The estimates in Eqs. (16) and (21) show that $\rho_{\Phi_1^2}\gg\rho_{\Psi_1^2},\rho_{\Phi_1\Psi_1}$.

IV. SECOND-HARMONIC VELOCITY PERTURBATION

The acoustic equation $L_{\xi_2}^{2a}=S_{\Phi_1^2}^a+S_{\Phi_1\Psi_1}^a$ has the form

$$\frac{(2\omega)^2}{v_A^2}\xi_2=\frac{1}{2B_0^2}(\mathbf{b}_0\cdot\nabla)(B_0^2\nabla F_1\cdot\nabla F_1)-\mathbf{b}_0\cdot\left[\nabla_\perp\frac{\nabla\cdot(B_0\nabla\Psi_1)}{B_0^2}\times\nabla F_1\right]. \tag{22}$$

The low β assumption does not allow us to discard ξ_2 immediately (as we did with ξ_1), since second-harmonic parallel velocity perturbations can arise from the nonlinear ponderomotive force (not associated with plasma pressure). Straightforward estimates of the two terms on the right-hand side of Eq. (22) give

$$\xi_2\sim\frac{m^2}{r^2Rq}\frac{\Phi_1^2}{B_0^2}\Rightarrow\rho_{\xi_2}\sim\frac{m^2}{r^2R^2q^2}\frac{\rho_0}{B_0^2}\Phi_1^2\ll\rho_{\Phi_1^2}. \tag{23}$$

These estimates show that ξ_2 can safely be neglected in calculating the perturbed density.

The second-harmonic compressional Alfvén wave equation reduces to $L_{\Psi_2}^{2c}+L_{\Phi_2}^{2c}=S_{\Phi_1^2}^c+S_{\Phi_1\Psi_1}^c$. To obtain an estimate for Ψ_2, we consider two possible ways of balancing this equation. If we first assume that $L_{\Psi_2}^{2c}\sim L_{\Phi_2}^{2c}$ we find $\Psi_2\sim\varepsilon^2/(m^2q^2)\Phi_2$ [which is similar to what follows from Eq. (13)], and the resulting density perturbation is relatively small ($\rho_{\Psi_2}\ll\rho_{\Phi_2}$). Alternatively, we can estimate Ψ_2 by assuming that $L_{\Psi_2}^{2c}=S_{\Phi_1^2}^c+S_{\Phi_1\Psi_1}^c$ or equivalently,

$$-\nabla\cdot(B_0\nabla\Psi_2)=-\frac{1}{2}B_0^2(\nabla F_1\cdot\nabla F_1)+\frac{1}{2}\mathbf{B}_0\cdot\left[\nabla\frac{\nabla\cdot(B_0\nabla\Psi_1)}{B_0^2}\times\nabla_\perp\Phi_1\right]. \tag{24}$$

The nonlinear terms on the right-hand side of this equation can be estimated as $S_{\Phi_1^2}^c+S_{\Phi_1\Psi_1}^c\sim m^4/(r^4R^2q^2)\Phi_1^2$, so that

$$\Psi_2\sim\frac{\Phi_1^2}{B_0R^2q^2}\Rightarrow\rho_{\Psi_2}\sim\frac{m^2}{r^2R^2q^2}\frac{\rho_0}{B_0^2}\Phi_1^2\ll\rho_{\Phi_1^2}. \tag{25}$$

Based on the above estimates, we neglect the Ψ_2 contribution to the perturbed density. As a result, Eq. (11) for the second-harmonic density perturbation simplifies to $\rho_2=\rho_{\Phi_2}+\rho_{\Phi_1^2}$.

In order to calculate ρ_{Φ_2}, we need to determine Φ_2 from the second-harmonic vorticity equation $L^{2v}=S^v$. When dealing with the source term $S^v_{\Phi_1^2}$, we must pay special attention to the cancellation of the $-4\pi\rho_0(\mathbf{v}_1\cdot\nabla)\mathbf{v}_1$ and $(\mathbf{B}_1\cdot\nabla)\mathbf{B}_1$ terms in a homogeneous plasma with straight magnetic field lines. The resulting second-harmonic vorticity equation has the form

$$4\frac{1}{r}\frac{d}{dr}\left(rD\frac{d\tilde{\Phi}_2}{dr}\right)-16\frac{m^2}{r^2}\tilde{\Phi}_2 D = \frac{m}{r\bar{B}_0}\left\{2\frac{dD}{dr}\left[\left(\frac{d\tilde{\Phi}_1}{dr}\right)^2-\frac{m^2}{r^2}\tilde{\Phi}_1^2\right] + D\left(\frac{d\tilde{\Phi}_1}{dr}\frac{d^2\tilde{\Phi}_1}{dr^2}-\tilde{\Phi}_1\frac{d^3\tilde{\Phi}_1}{dr^3}\right)-\bar{k}_\parallel\frac{d^2\bar{k}_\parallel}{dr^2}\frac{d\tilde{\Phi}_1^2}{dr}\right\}, \tag{26}$$

where $\Phi_2=\tilde{\Phi}_2(r)e^{2i(n\varphi-m\theta-\omega t)-i\pi/2}$. In deriving Eq. (26), flux surface averaging has been performed to eliminate the poloidal sidebands in S^v that are proportional to $\sin\theta$ or $\cos\theta$. These off-resonant sidebands produce only a small $2m\pm1$ correction to the dominant second-harmonic response.

Taylor expanding the coefficients in Eq. (26) around the zero shear point $r=r_\star$ to the second order enables us to transform Eq. (26) to

$$4\frac{d}{dx}(S+x^2)\frac{d\tilde{\Phi}_2}{dx}-16(S+x^2)\tilde{\Phi}_2+4Q_2\tilde{\Phi}_2 = 4x\left[\left(\frac{dT}{dx}\right)^2-T^2\right]+(S+x^2)\left(\frac{dT}{dx}\frac{d^2T}{dx^2}-T\frac{d^3T}{dx^3}\right)+\frac{d(T^2)}{dx}, \tag{27}$$

where $T(x)\equiv m\tilde{\Phi}_1/(r_\star\sqrt{\bar{B}_0})$ and S is the eigenvalue of the AC eigenmode equation [(18)]. The effects of hot ions and toroidicity have been added through the parameter Q_2, which is defined by replacing m and n by $2m$ and $2n$ in Eq. (20).

To illustrate the second-harmonic response, we choose a special case in which $Q_{\rm hot}\gg Q_{\rm tor}$. This assumption makes Q independent of the mode numbers and, consequently, we have $Q_1=Q_2=Q$. Figure 1 shows numerical solutions to Eq. (27) in the above limit for two different values of Q. It is essential that the values of the constant S in Eq. (27) are different from the eigenvalues of the linear operator on the left-hand side for both values of Q, ensuring uniqueness of the solutions. These solutions give $\Phi_2\sim T^2\sim m^2\Phi_1^2/(r^2B_0)$ when $Q\simeq0.65$. They also indicate that Φ_2 decreases with increasing Q.

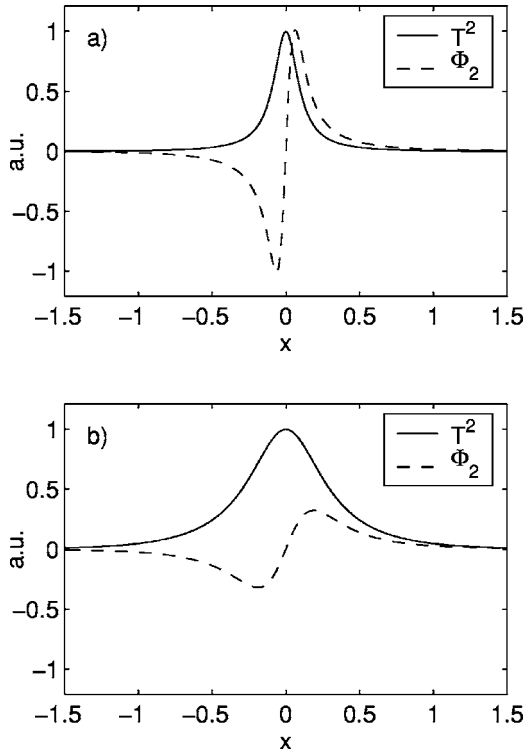

FIG. 1. Solution to Eq. (27) for (a) $Q=0.65$, $S=0.011$ and (b) $Q=1$, $S=0.10$. Note that the amplitude of Φ_2 decreases with increasing Q, and that $\tilde{\Phi}_2(x)$ is an odd function of x whereas $\tilde{\Phi}_1(x)$ is an even function of x.

V. SECOND-HARMONIC DENSITY PERTURBATION

The second-harmonic density perturbation generated by Φ_2 can be estimated as

$$\rho_{\Phi_2}=-\rho\nabla\Phi_2\cdot\left(\nabla\times\frac{\mathbf{b}_0}{B_0}\right)-\left(\frac{\mathbf{b}_0}{B_0}\times\nabla\Phi_2\right)\cdot\nabla\rho_0 \sim\left(\frac{1}{R}+(\ln\rho_0)'\right)\frac{m^3}{r^3}\frac{\rho_0\Phi_1^2}{B_0^2}, \tag{28}$$

which shows that ρ_{Φ_2} is larger than $\rho_{\Phi_1^2}$ in Eq. (21) by a factor $m\gg1$. However, the resonant enhancement becomes less efficient when Q increases because of the increasing frequency shift $\Delta\omega$ away from the Alfvén continuum and the concomitant widening of the first-harmonic radial profile. It is evident from the numerical solution shown in Fig. 1 that the amplitude of Φ_2 decreases with increasing Q. For $Q=1$, the amplitude of Φ_2 is already lower than T^2 by roughly a factor of 3. For larger values of Q this numerical factor may exceed the mode number m, making $\rho_{\Phi_1^2}$ comparable to or greater than ρ_{Φ_2} for high Q.

To compare ρ_2 with ρ_1 we need an estimate for the first-harmonic density perturbation, which can be obtained from Eq. (9),

$$\rho_1=-\rho\nabla\Phi_1\cdot\left(\nabla\times\frac{\mathbf{b}_0}{B_0}\right)-\left(\frac{\mathbf{b}_0}{B_0}\times\nabla\Phi_1\right)\cdot\nabla\rho \sim\left(\frac{1}{R}+(\ln\rho_0)'\right)\frac{m}{r}\frac{\rho_0\Phi_1}{B_0}. \tag{29}$$

For moderately large values of Q, the ratio ρ_2/ρ_1 is approximately of order

$$\frac{\rho_2}{\rho_1}\sim\frac{\rho_{\Phi_2}}{\rho_1}\sim\frac{m^2}{r^2}\frac{\Phi_1}{B_0}\sim\frac{mq}{\varepsilon}\frac{|\mathbf{B}_{\Phi_1}|}{B_0}. \tag{30}$$

This rough estimate only refers to the maximum values of ρ_1 and ρ_2, whereas locally the ratio of ρ_2 to ρ_1 can differ significantly from Eq. (30) as these two quantities have different radial and poloidal dependences.

VI. SUMMARY

The main results of this work are: (i) that the shear Alfvén perturbation is the dominant contributor to the second-harmonic density fluctuations produced by Alfvén cascades, and (ii) that the second-harmonic density perturbation can be calculated from Eqs. (21) and (28) by first solving Eq. (27), in which the radial profile of the AC eigenmode is known from Eq. (18). For moderate values of Q, the nonlinearity of the momentum balance equation is more important than the nonlinearity of the continuity equation and the resulting second-harmonic density is given by Eq. (28).

The above analysis can potentially be used to obtain more information about the AC out of experimental measurements. In particular, the fact that the ratio ρ_2/ρ_1 is proportional to the magnetic field of the basic harmonic perturbation [see Eq. (30)] points to the possibility of determining the AC amplitude inside the plasma, rather than just at the edge as with magnetic probes.

ACKNOWLEDGMENTS

We are grateful to Andrew Cole and James Van Dam for stylistic comments.

This work was supported by the European Community under an association contract between Euratom and Sweden, and by the U.S. Department of Energy Contract No. DE-FG03-96ER-54346.

[1] H. Kimura, Y. Kusama, M. Saigusa *et al.*, Nucl. Fusion **38**, 1303 (1998).
[2] S. E. Sharapov, D. Testa, B. Alper, D. N. Borba, A. Fasoli, N. C. Hawkes, R. F. Heeter, M. Mantsinen, M. G. Von Hellermann, and contributors to the EFDA-JET Workprogramme, Phys. Lett. A **289**, 127 (2001).
[3] R. Nazikian, G. J. Kramer, C. Z. Cheng, N. N. Gorelenkov, H. L. Berk, and S. E. Sharapov, Phys. Rev. Lett. **91**, 125003 (2003).
[4] H. L. Berk, D. N. Borba, B. N. Breizman, S. D. Pinches, and S. E. Sharapov, Phys. Rev. Lett. **87**, 185002 (2001).
[5] B. N. Breizman, H. L. Berk, M. S. Pekker, S. D. Pinches, and S. E. Sharapov, Phys. Plasmas **10**, 3649 (2003).
[6] A. Fukuyama and T. Akutsu, *Proceedings of the 19th International Conference on Fusion Energy 2002, Lyon, 2002* (IAEA, Vienna, 2003), TH/P3-14.
[7] J. A. Snipes, N. Basse, C. Boswell *et al.*, Phys. Plasmas **12**, 056102 (2005).
[8] B. D. G. Chandran, Astrophys. Space Sci. **292**, 17 (2004).
[9] B. N. Breizman, M. S. Pekker, and S. E. Sharapov, Phys. Plasmas **12**, 112506 (2005).